

HEATING THE BUBBLY GAS OF GALAXY CLUSTERS WITH WEAK SHOCKS AND SOUND WAVES

S. HEINZ^{1,2}, E. CHURAZOV^{3,4}

¹ CENTER FOR SPACE RESEARCH, MIT, 77 MASS. AVE., CAMBRIDGE, MA 02139

² CHANDRA FELLOW

³ MAX-PLANCK-INSTITUTE FOR ASTROPHYSICS, KARL-SCHWARZSCHILD-STR. 1, 85741 GARCHING, GERMANY

⁴ SPACE RESEARCH INSTITUTE (IKI), PROFSOYUZNAYA 84/32, MOSCOW 117810, RUSSIA

Draft version August 26, 2017

ABSTRACT

Using hydrodynamic simulations and a technique to extract the rotational component of the velocity field, we show how bubbles of relativistic gas inflated by AGN jets in galaxy clusters act as a catalyst, transforming the energy carried by sound and shock waves to heat. The energy is stored in a vortex field around the bubbles which can subsequently be dissipated. The efficiency of this process is set mainly by the fraction of the cluster volume filled by (sub-)kpc scale filaments and bubbles of relativistic plasma.

Subject headings: hydrodynamics — instabilities — shock waves — methods: numerical — galaxies: clusters: general — ISM: bubbles

1. INTRODUCTION

Models for the formation of galaxy clusters require an external source of energy to avoid catastrophic cooling of gas at the centers of massive clusters and to explain the observed lack of cool gas (Peterson et al. 2003) in so-called cooling flow clusters (Fabian 1994). Relativistic jets from supermassive black holes are the most likely source of this energy (Binney & Tabor 1995). While jets may carry sufficient kinetic energy, it has been unclear how efficiently that energy can be transferred to heat the cluster gas.

When jets interact with the gas in galaxy clusters (the intra-cluster medium, ICM), they invariably inflate hot, tenuous bubbles of relativistic gas, observed as synchrotron radio nebulae (Scheuer 1974), a.k.a. radio lobes. Evidence is mounting (Enßlin 1999; Bîrzan et al. 2004; Giovannini & Feretti 2004) that the ICM is littered with such bubbles, each of which starts out growing supersonically, driving a strong shock (Heinz et al. 1998) that efficiently heats the ICM it encounters. However, X-ray observations show that the expansion rapidly decelerates and most bubbles expand subsonically, therefore not producing strong shocks (Fabian et al. 2000; McNamara et al. 2000).

The bubbles themselves store a fraction of the initial jet energy, some of which can be transferred to the gas and dissipated during the bubble's slow, buoyant rise in the cluster atmosphere (Churazov et al. 2001; Begelman 2001). Another significant fraction of the jet energy is released in the form of sound and weak shock waves (Fabian et al. 2003a). In homogeneous media, dissipation of wave energy is determined by microscopic transport processes like viscosity or conduction, which are well known for unmagnetized plasmas. Realistically, though, the presence of even weak B -fields in the ICM can alter the transport coefficients, making estimates of the dissipation rate very uncertain. High values for the microscopic viscosity have been postulated as a way to dissipate the wave energy (Ruszkowski et al. 2004; Reynolds et al. 2005; Fabian et al. 2005).

In this letter we argue that the presence of filaments and bubbles of relativistic gas provides an efficient way to extract the wave energy and heat the ICM *even if* viscosity and thermal conduction are strongly suppressed. In §2 we review the process responsible for this dissipation, §3 presents the nu-

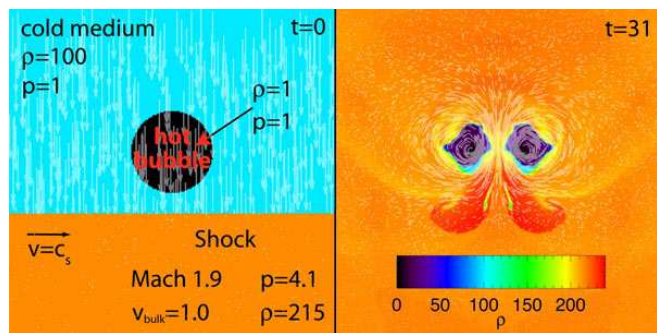


FIG. 1.— Map of fluid density (color scale) and velocity field (arrows) for Mach 1.9 shock running over a bubble with density contrast of 1:100. Shown are time frames 0 and 31 in units of the sound crossing time of the bubble.

merical methods we used, §4 discusses how our results can be applied to cluster heating, and §5 summarizes.

2. THE RICHTMYER-MESHKOV INSTABILITY

The energy transfer to the ICM occurs through a process known as the Richtmyer-Meshkov instability (RMI Richtmyer 1960; Meshkov 1969; Quirk & Karni 1996; Inogamov 1999). A plane shock or sound wave passing over a density discontinuity that is inclined with respect to the wave front, as it occurs at the boundary of the ICM with a relativistic bubble, induces a well-localized vortex flow around the bubble (Enßlin & Brüggén 2002), as illustrated in Fig. 1. A qualitatively similar process occurs when a shock passes over *overdense* clouds (Klein et al. 1994; Kornreich & Scalo 2000).

Because the high sound speed keeps the material inside the bubble at uniform (but time varying) pressure, the bubble acts like a hydraulic piston, distributing pressure applied at one end over its entire surface. The arrival of the wave sets up a pressure gradient which accelerates the bubble/wave interface inward, introducing significant *inward* transverse motion and distorting the bubble. *Ahead* of the wave, the overpressured bubble expands into the ICM, inducing significant *outward* transverse motion. Once the shock front has passed over the bubble, it leaves behind a vortex ring in what was previously irrotational flow. For a compression wave of finite

width λ , the passage of the trailing end of the wave will act in the opposite sense, partly restoring the bubble's original shape and canceling previously generated vorticity. This reduces the amount of energy deposited by the wave if λ is not large compared to the bubble radius R .

In the limit of low bubble density $\rho_{\text{bubble}} \ll \rho_{\text{ICM}}$, and for $R \ll \lambda$, one can easily estimate the amount of the energy funneled into this vortex: Material of density ρ_{ICM} enters the bubble volume V_{bubble} with velocity v_{ICM} (the bulk velocity of the compressed gas). Thus, the energy trapped in the toroidal vortex should be

$$E_{\text{rot}} = g \frac{1}{2} V_{\text{bubble}} \rho_{\text{ICM}} v_{\text{ICM}}^2 \quad (1)$$

where g depends on the bubble's geometry and should be of order unity for spherical bubbles. This energy is extracted from the wave and available for dissipation in the ICM.

In order to verify the dimensional analysis that leads to eq. (1) and to calibrate the coefficient g , we undertook a set of numerical hydrodynamic simulations of shock-bubble interactions. We shall present the details of our numerical study before discussing the results.

3. NUMERICAL METHOD

We performed multiple parameter studies of shock-bubble interactions. The setup consisted of a hot bubble of varying geometry embedded in a colder, denser medium. Shocks or non-linear sound waves of varying finite width λ and pulse height (i.e., Mach number) were introduced to travel across the bubble.

The simulations were carried out using the publically available FLASH code (Fryxell et al. 2000). FLASH is an adaptive mesh refinement hydrodynamics code that uses a second order accurate piece-wise parabolic solver. Most of our simulations were carried out on a 2D Cartesian grid with an effective grid size of 2048x3072 cells and an effective resolution of 64 cells across the bubble.

Figure 1 shows a typical setup with a density contrast of 100 and pressure balance across the bubble, the ratio of sound speeds is 10 from inside to outside of the bubble. We assumed an adiabatic equation of state except for the shock, which is handled implicitly by a shock capturing scheme. The ratio of specific heats for both hot and cold fluids was $\gamma = 5/3$. While this will not affect the results qualitatively, a softer $\gamma = 4/3$ equation of state would increase the compressibility of the bubble and lead to a slightly higher value of g .

In most of the simulations the shock was taken to be a semi-infinite piston with a sharp discontinuity in pressure, density and velocity, satisfying the Rankine-Hugoniot shock jump conditions, Landau & Lifshitz 1987. In the case of finite pulse width λ (Fig. 2), the initial pulse profile was taken to be a top-hat function in all fluid variables.

Our choice of grid implies a cylindrical bubble geometry. To confirm that our conclusions are independent of geometry we ran test-cases of spherical bubbles on a 2D axi-symmetric grid. A resolution study confirmed that our simulations are independent of numerical resolution. The results are insensitive to the bubble/environment density ratio $\rho_{\text{bubble}}/\rho_{\text{ICM}}$ as long as $\rho_{\text{bubble}} \ll \rho_{\text{ICM}}$. While the enforced symmetry of our 2D simulations might slightly alter the amount of vorticity generated and thus the numerical coefficient g , it has been shown that the RMI does operate in 3D and the results of this paper will most likely not be affected severely by restricting the analysis to 2D.

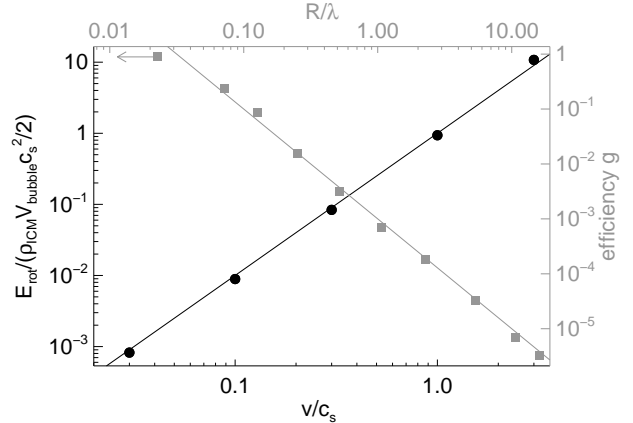


FIG. 2.— Black: Kinetic energy in the rotational velocity field extracted from sound/shock wave as a function of the bulk velocity of the shocked gas, v_{ICM} . Points correspond to Mach numbers $M = 1.02, 1.07, 1.22, 1.87, 4.20$. Grey: Energy extraction efficiency g as function of pulse width λ (relative to maximal value $g = 0.97$ for $\lambda \rightarrow \infty$).

The rotational component of the velocity field was extracted by solving the vorticity equation $\nabla \times \mathbf{v} = \nabla \times (\nabla \times \mathbf{A})$ for the vector potential \mathbf{A} (which reduces to Poisson's equation for $-A$ in 2D Cartesian coordinates), subject to the boundary condition of vanishing rotational velocity at infinity, making v_{rot} invariant under Galilean transformation. We used a Fast Fourier Transform method to solve the equation numerically. We then calculated the kinetic energy $E_{\text{rot}} = \int dV \rho (\nabla \times \mathbf{A})^2 / 2$ contained in the rotational part of the flow. The potential velocity field can be found by solving Poisson's equation $\nabla^2 \phi = \nabla \cdot \mathbf{v}$.

4. DISCUSSION

4.1. Numerical calibration of g

These simulations can be used to test eq. (1) and to calibrate the numerical coefficient g . Fig. 2 shows the kinetic energy E_{rot} in rotational flow as a function of v_{ICM} in the limit $R \ll \lambda$. The numerical results are in good agreement with the estimate from eq. (1), with a numerical fit of $g = 0.97$. Fig. 2 also shows that for $\lambda \lesssim 10R$, g is proportional to $(\lambda/R)^2$. This dependence of g on λ/R is linked to the degree of bubble deformation produced during shock passage. Because the total amount of energy in the wave is proportional to λ , the energy transfer efficiency is $\eta = g(R/\lambda) \propto \lambda/R$. Thus, small bubbles are more efficient at extracting energy than large ones.

Bubble shape and orientation also affect g : Fig. 3 shows that E_{rot} depends on w and l , the bubble's dimensions parallel and perpendicular to the wave. The numerical fit for aspect ratios l/w not too far from unity is $g \propto (l/w)^{0.8}$: the more surface area the bubble presents to the wave relative to its volume, the less efficient the mechanism becomes. The dependence of g on filament orientation shown in Fig. 3 (grey) is due to the effective aspect ratio changing with angle. This dependence can be easily understood considering that all effects essential for deposition of rotational energy into the ICM (vorticity generation and bubble deformation) scale with the length l of the filament perpendicular to the front.

4.2. Application to galaxy clusters

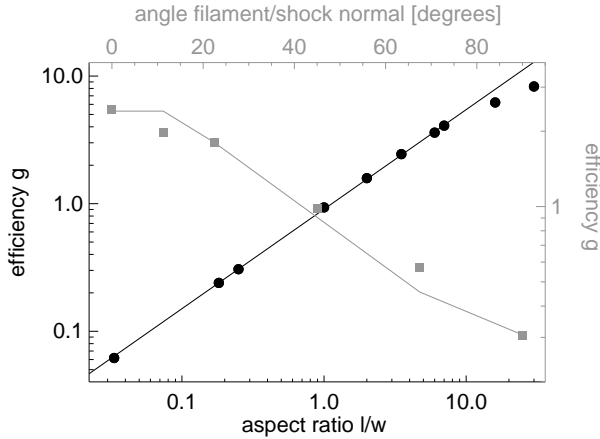


FIG. 3.— Extraction efficiency g for kinetic energy in rotational flow as a function of aspect ratio l/w (black circles) of the filament and best fit regression of $g \propto (l/w)^{0.8}$ (black line). Bubbles exposing *less* surface area to the shock are *more* efficient at extracting energy per unit bubble volume. Also shown: Efficiency g as a function of angle between filament and shock normal for an aspect ratio of $l/w = 3.5$ (grey squares) and expected dependence $g \propto (\Delta y/\Delta x)^{0.8}$ from measured x- and y-cuts across the filament (grey line).

These results imply that a distribution of bubbles of hot gas whose characteristic size is small compared to their distance r from the cluster center can extract energy from a sound or shock wave passing over them rather efficiently. The total energy captured equals the energy density in the wave times the volume filled by bubbles. To demonstrate this, Fig. 4 shows a simulation of a random distribution of bubbles (filling about 10% of the volume) before and after the shock passage. The top panels show the creation of a turbulence field around the bubbles in the wake of the shock. The bottom panel shows the decomposition of the velocity field into rotational and potential flow. E_{rot} and the viscous dissipation rate are well localized around the bubbles even long after the shock passage.

The velocity in the differentially rotating vortices drops with distance from the bubble center and a number of dissipative processes (such as the magneto-rotational instability (Balbus & Hawley 1991), turbulence, and microscopic viscosity) will dissipate the energy contained in the vortex. The dissipated heat and entropy will go directly into the thermal gas surrounding the bubble. Since small bubbles rise through the cluster gas with speeds much smaller than the sound speed (Churazov et al. 2002), the deposition of rotational energy and the subsequent heating occur at an essentially fixed location in the cluster compared to the passing wave.

Whether the condition $R \ll \lambda$ is satisfied in galaxy clusters depends on the unknown size distribution of bubbles in the ICM. In sub-sonic models of ICM heating (Begelman 2001; Churazov et al. 2002) it is typically assumed that a large number of small bubbles is released rather than few large bubbles. X-ray and radio images of nearby clusters indicate that the distribution of radio plasma can be rather complex (Owen et al. 2000; Young et al. 2002; Fabian et al. 2003a), though resolution limits and the line of sight projection in X-ray and radio maps make a direct detection of small filaments impossible. The bubbles detected directly in these clusters are of similar size to the sound waves seen, implying a low energy extraction efficiency g . In addition to these prominent,

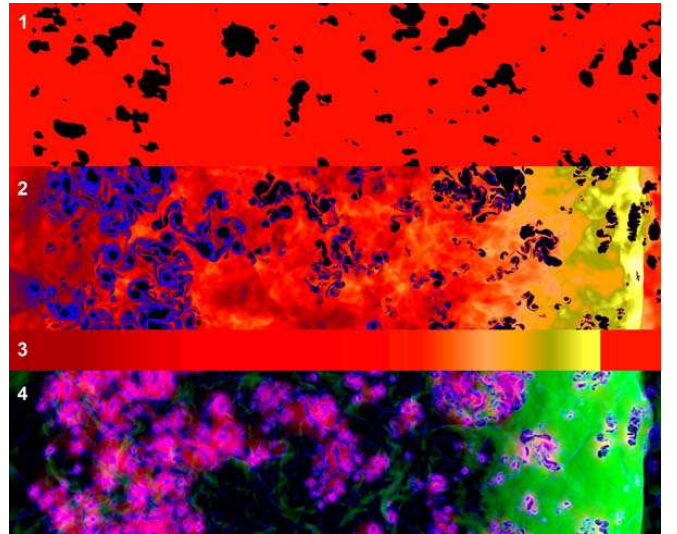


FIG. 4.— Random distribution of low density bubbles (filling fraction $f = 10\%$) before (panel 1) and after (panel 2) passage of an initially square pulse of Mach 1.87, which induces a complex turbulence field in the wake of the bubbles and distorts the wave front, compared to the same setup but with uniform density (panel 3). Panel 4: Kinetic energy of the decomposed velocity field: rotational flow (red); potential flow (sound/shock waves, green); and viscous dissipation rate (blue, in units of specific viscosity). Note that the rotational energy is localized around regions of enhanced bubble number density and that some of the energy in potential flow is radiated away in sound waves.

large radio bubbles, radio observations of clusters also show more amorphous radio halos (e.g. Pedlar et al. 1990), extending over the central ~ 100 kpc. Such halos *could* indicate that smaller radio bubbles/filaments are present in the ICM.

Dynamical (Rayleigh-Taylor and Kelvin-Helmholtz) instabilities (Landau & Lifshitz 1987) lead to fragmentation and shredding of individual bubbles, producing a spectrum of smaller filaments. In the absence of magnetic fields, buoyantly rising bubbles are shredded into smaller structures while passing a distance comparable to their own diameter, within a time scale $\tau_{\text{shred}} \sim 2 \times 10^7 \text{ yrs} \sqrt{(R/10 \text{ kpc})(4 \text{ keV}/T)}$ for a cluster of temperature T . As long as τ_{shred} is comparable to or smaller than the buoyant rise time $\tau_{\text{buoy}} \sim 5 \times \tau_{\text{shred}} [(r_{\text{cool}}/100 \text{ kpc})(10 \text{ kpc}/R)]^{3/2}$ a significant fraction of a bubble's volume will be shredded within the cluster's cooling radius r_{cool} . A more quantitative evaluation of bubble shredding, including the effects of the magnetic fields and viscosity, which can significantly suppress the shredding efficiency, is a topic of ongoing research (Reynolds et al. 2005; Kaiser et al. 2005) and beyond the scope of this paper.

Shredding bubbles to smaller sizes increases the efficiency g until they reach a characteristic size much smaller than the wave length of the perturbations. After this point, g is unaffected by bubble size, though the buoyant rise velocity still decreases with bubble size, thus leaving more and more time for dissipation processes to act on the vorticity field. Ultimately, if bubbles get shredded to small enough sizes their relativistic gas content might get microscopically mixed with the ICM. The energy contained in the low energy electrons can then also contribute to ICM heating via Coulomb losses.

As a possible application of the process suggested above, consider the Perseus cluster, one of the brightest cooling flow clusters. The size of the prominent central radio bubbles is about 10 kpc. This sets the typical thickness of $\lambda \sim 10$

kpc of the waves generated by bubble inflation, consistent with the concentric ripples seen in X-ray images (Fabian et al. 2003a). Since the bubbles are comparable in size to λ , they are inefficient at extracting energy from AGN induced sound waves. However, if the ICM in Perseus is filled with numerous smaller bubbles, the typical attenuation length for a compression wave will be $L \sim \lambda/f$, where f is the fraction of cluster volume filled by bubbles. For $f \sim 10\%$, most of the wave energy would be trapped in the inner ~ 100 kpc of the cluster, where most of the excess heating is required. Values of f up to 10% might be reasonable if a significant fraction of the radio plasma seen in cluster cavities with $R \sim \lambda$ (Birzan et al. 2004; Giovannini & Feretti 2004) is shredded to smaller scales, or if the radio plasma producing the diffuse cluster radio halo is filamentary rather than homogeneous.

Thus, even in the absence of microscopic viscosity, a bubbly ICM can prevent leakage of wave energy out of the central region. Moreover, bubbles will also boost the dissipation of sound waves created by other mechanisms (e.g., cluster collisions) in the central region, where f is presumably largest. Generally, filling factors of $f \sim \text{few}\% - \text{few} \times 10\%$ are necessary to provide the required heating in cooling flow clusters.

4.3. Strong shocks in the cluster center

Recent deep cluster observations have revealed large scale surface brightness discontinuities that are consistent with moderate strength shocks (McNamara et al. 2005; Nulsen et al. 2005). This could mean that cluster centers are subject to much stronger shocks than the cool X-ray rims around radio bubbles would imply. The question of why strong, jet driven shocks have not been found has been a puzzle ever since *Chandra* began observing the temperature

structures of the inner regions of galaxy clusters. The presence of bubbles in the ICM might help explain the lack of observational evidence for such shocks: the large sound speed inside the bubbles means that they rapidly broadcast the arrival of a shock, which locally jumps ahead when passing over a filament. This not only scatters some of the shock into isotropic sound waves, it also distorts and broadens the front (Fig. 4). When observing such a shock in X-rays it will appear weaker than a coherent shock in the absence of bubbles.

Such strong shocks might be efficient enough to heat the cluster directly. However, the presence of bubbles increases the dissipation efficiency *regardless* of shock strength. Therefore, the proposed mechanism would still operate.

5. CONCLUSIONS

The presence of bubbles of relativistic gas in galaxy clusters can provide a significant boost to the efficiency with which shock and sound waves energize the gas. Given the ubiquity of both sound waves and of relativistic gas in galaxy clusters, this may well be a significant (if not dominant) channel of cluster gas heating. More generally, our results demonstrate the high efficiency of the RMI, which is known to have a broad range of scientific and industrial applicability.

Acknowledgements: We would like to thank Emily Levesque and Thomas Janka for helpful discussions. SH acknowledges support by the National Aeronautics and Space Administration through Chandra Postdoctoral Fellowship Award Number PF3-40026 issued by the Chandra X-ray Observatory Center, which is operated by the Smithsonian Astrophysical Observatory for and on behalf of the National Aeronautics Space Administration under contract NAS8-39073.

REFERENCES

- Birzan, L., Rafferty, D. A., McNamara, B. R., Wise, M. W., & Nulsen, P. E. J. 2004, *ApJ*, 607, 800
- Balbus, S. A. & Hawley, J. F. 1991, *ApJ*, 376, 214
- Begelman, M. C. 2001, in *ASP Conf. Ser. 240: Gas and Galaxy Evolution*, 363–+
- Binney, J. & Tabor, G. 1995, *MNRAS*, 276, 663
- Churazov, E., Brüggén, M., Kaiser, C. R., Böhringer, H., & Forman, W. 2001, *ApJ*, 554, 261
- Churazov, E., Sunyaev, R., Forman, W., & Böhringer, H. 2002, *MNRAS*, 332, 729
- Enßlin, T. A. 1999, *Diffuse Thermal and Relativistic Plasma in Galaxy Clusters*, 275
- Enßlin, T. A. & Brüggén, M. 2002, *MNRAS*, 331, 1011
- Fabian, A. C. 1994, *ARA&A*, 32, 277
- Fabian, A. C., Reynolds, C. S., Taylor, G. B., & Dunn, R. J. H. 2005
- Fabian, A. C., Sanders, J. S., Allen, S. W., Crawford, C. S., Iwasawa, K., Johnstone, R. M., Schmidt, R. W., & Taylor, G. B. 2003a, *MNRAS*, 344, L43
- Fabian, A. C., Sanders, J. S., Ettori, S., Taylor, G. B., Allen, S. W., Crawford, C. S., Iwasawa, K., Johnstone, R. M., & Ogle, P. M. 2000, *MNRAS*, 318, L65
- Fryxell, B., Olson, K., Ricker, P., Timmes, F. X., Zingale, M., Lamb, D. Q., MacNeice, P., Rosner, R., Truran, J. W., & Tufo, H. 2000, *ApJS*, 131, 273
- Giovannini, G. & Feretti, L. 2004, *Journal of Korean Astronomical Society*, 37, 323
- Heinz, S., Reynolds, C. S., & Begelman, M. C. 1998, *ApJ*, 501, 126
- Inogamov, N. A. 1999, *Astrophysics and Space Physics Reviews*, 10, 1
- Kaiser, C. R., Pavlovski, G., Pope, E. C. D., & Fangohr, H. 2005, *MNRAS*, 359, 493
- Klein, R. I., McKee, C. F., & Colella, P. 1994, *ApJ*, 420, 213
- Kornreich, P. & Scalo, J. 2000, *ApJ*, 531, 366
- Landau, L. D. & Lifshitz, E. M. 1987, *Fluid Mechanics* (Oxford England, New York: Pergamon Press)
- McNamara, B. R., Nulsen, P. E. J., Wise, M. W., Rafferty, D. A., Carilli, C., Sarazin, C. L., & Blanton, E. L. 2005, *Nature*, 433, 45
- McNamara, B. R., Wise, M., Nulsen, P. E. J., David, L. P., Sarazin, C. L., Bautz, M., Markevitch, M., Vikhlinin, A., Forman, W. R., Jones, C., & Harris, D. E. 2000, *ApJ*, 534, L135
- Meshkov, E. E. 1969, *Sov. Fluid. Dyn.*, 4, 101
- Nulsen, P. E. J., Hambrick, D. C., McNamara, B. R., Rafferty, D., Birzan, L., Wise, M. W., & David, L. P. 2005, *ApJ*, 625, L9
- Owen, F. N., Eilek, J. A., & Kassim, N. E. 2000, *ApJ*, 543, 611
- Pedlar, A., Ghataure, H. S., Davies, R. D., Harrison, B. A., Perley, R., Crane, P. C., & Unger, S. W. 1990, *MNRAS*, 246, 477
- Peterson, J. R., Kahn, S. M., Paerels, F. B. S., Kaastra, J. S., Tamura, T., Bleeker, J. A. M., Ferrigno, C., & Jernigan, J. G. 2003, *ApJ*, 590, 207
- Quirk, J. J. & Karni, S. 1996, *Journal of Fluid Mechanics*, 318, 129
- Reynolds, C. S., McKernan, B., Fabian, A. C., Stone, J. M., & Vernaleo, J. C. 2005, *MNRAS*, 357, 242
- Richtmyer, R. D. 1960, *Comm. Pure Appl. Math.*, 8, 297
- Ruszkowski, M., Brüggén, M., & Begelman, M. C. 2004, *ApJ*, 611, 158
- Scheuer, P. A. G. 1974, *MNRAS*, 166, 513
- Young, A. J., Wilson, A. S., & Mundell, C. G. 2002, *ApJ*, 579, 560